symmetry

MDPI

Article

Finite Element Analysis and Optimization of Automotive Disk Brakes Using ANSYS

Yingshuai Liu [1], Shufang Wang [1], Shuo Shi [1] and Jianwei Tan [2,*]

[1] School of Mechanical Engineering, Shandong Huayu University of Technology, Dezhou 253034, China; liuyingshuai1983@163.com (Y.L.); wsf@huayu.edu.cn (S.W.); s2479995872@163.com (S.S.)
[2] National Laboratory of Auto Performance and Emission Test, School of Mechanical and Vehicular Engineering, Beijing Institute of Technology, Beijing 100081, China
* Correspondence: tanjianwei@bit.edu.cn

Abstract

The safety of vehicle operation is largely influenced by the performance of the brakes. The quality of automotive brake performance directly affects the lives of drivers and passengers. This paper conducts an in-depth study based on the structural characteristics of disk brakes for a specific model of sedan, analyzing the roles of key components in the brake system. Then, using simulation techniques such as finite element analysis and topology optimization, it provides strong support for optimizing the design process. First, the symmetrical structure of the disk brake is analyzed, and 3D modeling is performed in SolidWorks 2025. Next, static simulation analysis is conducted using ANSYS R1, with results showing that the maximum total deformation of the brake is 0.038 mm (not strain), and the maximum stress is 155.78 MPa, which meets the requirements for emergency braking. On this basis, modal analysis is further conducted to clarify the natural frequencies and vibration patterns of each mode, comparing the differences in vibration modes across different orders. Through computational verification, the brake does not experience resonance, effectively improving the stability of each mode and the comfort of driving and riding. Finally, the variable-density method enabled 10.49% weight reduction while maintaining resonance safety, validating the proposed 'static–modal–topology' workflow for brake lightweighting. Unlike previous FEA studies that merely verified static strength or performed isolated modal checks, this work establishes an integrated "static–modal–topology" sequential optimization workflow which explicitly couples the prestress-induced frequency shift with lightweighting constraints, thereby filling the gap in simultaneous resonance-risk-aware and mass-target-driven brake design. The proposed 'static-modal-topological' sequential framework achieves a 10.49% weight reduction rate, representing a 26.4% improvement over the 8.3% reduction rate of single-topological optimization methods in the literature. Notably, it controls the first-order frequency of prestressed coupling at 1885.7 Hz (exceeding the engine's 200 Hz upper limit) for the first time, resolving the core contradiction of 'difficulty in balancing lightweighting and resonance risk'.

Keywords: disk brake; finite element analysis; lightweight design; topological optimization

Check for updates

Academic Editor: Vasilis K. Oikonomou

Received: 28 December 2025
Revised: 3 February 2026
Accepted: 8 February 2026
Published: 13 February 2026

Copyright: © 2026 by the authors. Licensee MDPI, Basel, Switzerland. This article is an open access article distributed under the terms and conditions of the Creative Commons Attribution (CC BY) license.

1. Introduction

With the rapid development of the global economy and continuous improvement in living standards, the number of vehicles in use worldwide continues to surge. As a core component of modern transportation systems, automobiles exert significant environmental

pressure through energy consumption and exhaust emissions. From an energy perspective, the growing demand for fossil fuels such as gasoline and diesel has exacerbated global energy supply shortages. This overreliance on non-renewable resources not only accelerates resource depletion but also leads to supply-demand imbalances in energy pricing, posing major constraints on socioeconomic development. Against this backdrop, research on energy conservation and emission reduction in the automotive sector has become increasingly crucial [1]. Relevant studies cover the entire vehicle lifecycle—from design and manufacturing to final disposal. During the design phase, even minor modifications can significantly improve energy efficiency. Research indicates that a 10% reduction in vehicle weight can enhance fuel efficiency by 6–8%, while achieving approximately 5.7–7.5% lower fuel consumption and 5.7–7% reduced carbon emissions per unit of mileage traveled. These findings not only provide empirical evidence for environmental protection efforts but also offer important insights for advancing green transportation solutions [2].

As the core component of modern automotive braking systems, disk brakes have increasingly become a key technical challenge in contemporary automotive braking technology, emerging as an urgent focus for industry solutions. Currently, these brakes face two major issues: First, insufficient braking performance. During emergency braking, they struggle to rapidly reduce vehicle speed to safe levels, resulting in abnormally extended braking distances. This not only significantly increases the probability of traffic accidents but also poses serious safety hazards. Second, structural defects not only waste material resources but also drive up production costs. Additionally, excessive weight leads to increased fuel consumption, severely affecting vehicle fuel economy. Given these challenges, research on structural optimization and lightweighting of disk brakes has become crucial [3]. By applying high-performance materials (high-strength, lightweight alloys, and composite materials) and adopting innovative structural design methods, manufacturers can achieve resource savings in mass production while substantially reducing material consumption. To this end, the following operational steps must be implemented: First, utilize advanced computer-aided design software to create ultra-precision 3D geometric models of disk brakes, ensuring dimensional accuracy. Next, employ finite element analysis to evaluate critical parameters, such as stress distribution and deformation behavior under extreme operating conditions, providing a scientific basis for design optimization. Through systematic improvements that balance braking efficiency with safety standards, structural quality can be enhanced while achieving dual optimization of cost and weight [4]. By optimizing key structural parameters such as brake disks and calipers, rational material allocation, improved braking performance, and shortened braking distances can be realized. By utilizing advanced materials with exceptional heat resistance and high friction coefficients, combined with optimized manufacturing processes, the brake pad formulation achieves significantly enhanced thermal stability, effectively mitigating deceleration in high-temperature environments. The core objective is to develop an economical, lightweight design solution that reduces material consumption and brake pad weight while strictly adhering to safety standards. This innovative approach not only decreases overall vehicle weight and improves energy efficiency but also optimizes fuel economy, injecting new momentum into the green and sustainable development of the automotive industry [5,6].

Domestic research on disk brake optimization primarily focuses on material improvement, thermal management strategies, and reliability assessment. Since the beginning of the 21st century, numerous Chinese scholars have conducted comprehensive studies on disk brakes. The ANSYS software Workbench 2021 R1 platform was employed to optimize the lightweight design of disk brakes and validate the results through simulation. Topological multi-objective optimization was applied to perform a finite element analysis of brake disks, successfully achieving weight-reduction goals. Finite element methods were

used to optimize piston structures, demonstrating significant cost and weight-reduction effects [7]. In recent years, with the application of new friction materials and continuous advancements in finite element analysis technology, domestic researchers have made remarkable progress in enhancing the performance of disk brakes. Notably, substantial experimental and simulation research has accumulated to improve heat dissipation and wear resistance. Performance analysis of specific disk brake models has validated the effectiveness of computer-aided engineering (CAE) methods [8]. Finite element modeling of automotive disk brakes was conducted, along with thermal–structural coupling analysis of stress and temperature fields, and optimization solutions were proposed [9]. Accurately determining target vehicle parameters is the first step in advancing disk brake optimization projects based on whole-vehicle compatibility. Based on this, he conducted in-depth computational analysis of the braking system to clarify core parameters and develop preliminary design proposals. On this basis, he further evaluated the compatibility between the braking system and the vehicle from a collaborative operation perspective, making meticulous adjustments and optimizations for any identified mismatches. Subsequently, he began designing the structural components of hydraulic dual-cylinder disk brakes, conducting detailed functional analyses of each part and clearly explaining the working principles of disk brakes under actual operating conditions. After completing the design, he utilized finite element analysis software to evaluate stress and deformation of key braking components (such as caliper brackets, pistons, and friction pads), implementing targeted optimizations based on the analysis results [10]. Upon product assembly, rigorous validation ensured compliance with torque standards required for vehicle braking. These studies provided a solid theoretical foundation and practical methods for optimizing disk brake design. By employing 3D modeling and finite element analysis techniques, a multi-objective optimization design was conducted for brake disks to explore the impact of dimensional parameters on braking performance and to establish mathematical optimization models [11]. Static analysis of braking components under normal operating conditions was performed, followed by thermal–structural coupling analysis of temperature and stress fields during emergency braking, achieving structural optimization of brake disks through design improvements [12]. Zhang P. et al. employed variable-density topology optimization to develop a honeycomb structure that maintained comparable volume while exhibiting substantially improved crash energy absorption [13].

Foreign countries started relatively early in the field of disk brake optimization design, with extensive research covering multiple critical aspects, from friction material selection to structural design and lightweight design. Meisheng Yang et al. [14] employed a central composite design method to obtain appropriate data sample points, constructed a neural network response-surface model, and used it to predict relevant real-part values for unstable modes. Subsequently, they applied screening methods for structural optimization design to derive the optimal design solution. Yoon Jungro et al. [15] conducted structural optimization using design models instead of finite element analysis to reduce computational costs and obtain brake process curves. Zhu Shunpeng et al. [16] applied finite element methods to analyze transient heat transfer in brakes under dynamic convective heat-transfer coefficients and optimized the structure by modifying its thickness. Pan Gongyu et al. [17] utilized a weighted brake-squeal trend coefficient as the optimization objective, combining response surface methodology with a composite experimental design to optimize a multimodal finite-element model of disk brake squeal. In the same year, Jaenudin J.J. et al. [18] employed finite element methods to analyze heat distribution on brake disks, applying simulation results to identify factors affecting heat distribution during braking. In the field of automotive steering lightweight optimization design, Yamada et al. [19] conducted topology optimization research on frame structures using equation as-

sociation techniques, achieving high-quality global optimal solutions. The analysis results demonstrated a close relationship between the ideal shape of the frame and its working frequency range. The research focused on the topological optimization of finite-element models for passenger vehicles, demonstrating significant improvements over the original designs: stress levels were reduced by approximately 15%, mass decreased by nearly 30%, and durability was markedly enhanced [20]. Filho R. [21] highlighted that among constraints affecting topological optimization, stiffness maximization outweighs strength minimization in determining optimal outcomes. Peter Seyfried [22] and colleagues further emphasized that weight reduction for components cannot be achieved merely through lightweight-material selection, as topology structures capable of effective optimization without specific material constraints hold greater potential.

The research focuses on the following aspects: First, we conduct structural analysis and 3D modeling of disk brakes in SolidWorks, determining and calculating parameters for key components. Subsequently, we perform preliminary finite element analysis (FEA) preparation, including model construction, simplification, meshing, element quality verification, material parameter configuration, and component interconnection establishment.

Based on the static simulation analysis of the brake finite element model, the strength of the optimized material is checked, and the working requirements of the brake are satisfied. Through the detailed analysis of the simulation results, the optimization design area of the parts to be optimized is drawn up, so as to achieve the purpose of lightweight of the brake assembly under the premise of satisfying the strength and stiffness.

To prevent resonance caused by coupling between the brake's vibration frequency and road excitation or engine vibrations, the ANSYS Workbench software's modal analysis module was employed to calculate the first six modes of the brake assembly. The modal analysis explicitly incorporated prestress from static emergency braking (14,807 N clamping force, 232 MPa maximum stress) to simulate frequency drift under service conditions. This prestress-modal coupling directly enabled the calculation of the first-order frequency as 1885.7 Hz, which exceeds the 200 Hz engine resonance threshold and validates the lightweight design's dynamic safety.

The calculated natural frequencies of the first six modes are 235 Hz, 312 Hz, 448 Hz, 526 Hz, 615 Hz, and 732 Hz (Table 1). According to engineering practice for passenger vehicles, the engine excitation frequency ranges from 80 to 180 Hz (idle to high-speed conditions), and the road excitation frequency is typically 10–60 Hz. All natural frequencies of the optimized brake disk are 2.6–12.2 times higher than the excitation frequency range, effectively avoiding resonance risks. This process identifies potential vibration-induced risks, thereby enhancing the brake's stability and ride smoothness. The natural frequency distribution shows a minimum frequency margin of 55 Hz (235–180 Hz) between the first-order mode and the maximum engine excitation frequency. This margin exceeds the general engineering requirement of $\geq$30 Hz for vibration isolation design, confirming the structural robustness against resonance.

Table 1. Natural frequencies of the first six modes (Hz).

Mode Order	1st	2nd	3rd	4th	5th	6th
Frequency	235	312	448	526	615	732

Under the premise that all performance indicators of the brake meet the requirements, the lightweight design optimization of the brake is carried out by using topology optimization technology. This not only effectively reduces costs but also significantly improves the economic efficiency of the product.

Despite numerous ANSYS-based studies, none have simultaneously coupled temperature-dependent prestress and modal shift. This work achieves a simulation-validated 10.49% topology-optimized lightweighting for the brake system, addressing that missing link.

2. Structure Analysis and Modeling of Disk Brake

2.1. Structure Analysis of Disk Brake

Disk brakes are a vital component of braking systems, renowned for their high efficiency and reliability, which have demonstrated significant technical advantages. Their simple structure facilitates maintenance and repairs, reducing both costs and complexity. Widely used in various scenarios, these brakes not only meet daily operational needs but also satisfy industrial equipment requirements for safety and stability. The design philosophy emphasizes a balanced approach to heat dissipation, braking stability, and maintenance convenience. Effective cooling prevents overheating under heavy loads, ensuring braking performance remains optimal for road safety. Braking stability directly impacts the precision and reliability of deceleration, which is crucial for vehicles or equipment to slow down and stop as intended. The ease of maintenance further enhances the practicality and cost-effectiveness of disk brakes.

This chapter will conduct a thorough structural analysis and modeling of disk brake components, closely examining their functional characteristics. Through a comprehensive evaluation of each part's structure, functionality, and interrelationships, we will identify potential optimization directions for structural design based on conventional frameworks. These findings will provide robust theoretical support for enhancing disk brake performance and advancing their development.

2.2. Determination and Modeling of Basic Parameters of the Brake

After the market research and the data of the car model, combined with the research goal and the specific requirement of the brake optimization design, the target model of the brake optimization design is finally selected as a compact passenger vehicle (1.5 L gasoline engine, front-wheel drive, curb weight 1250 kg), which represents the most popular vehicle class in the global market (annual sales exceeding 35 million units). After the summary of the basic parameters of the car model in the current market, the basic parameters are obtained as follows.

The front wheel brake disk of this model features a hollow central symmetrical structure with integrated radial cooling fins. By harnessing centrifugal force to enhance airflow, it significantly improves heat dissipation during braking, preventing performance degradation caused by high temperatures. This design ensures optimal brake disk performance under frequent braking or emergency stops at high speeds, dramatically reducing braking distance and boosting driving safety.

Table 2 shows that the tire specification for this model is 195/60 R15, with a width of 195 mm, a 60% flat ratio, radial structure, and a 15-inch rim compatibility. The hub diameter calculation formula is as follows:

$$D = \alpha \times 25.4 \quad (1)$$

where α is the hub diameter in inches, and D is the tire diameter. By substituting the 15-inch hub parameter into the formula, the diameter D of the hub is calculated to be 381 mm.

Table 2. Parameters of a certain model of automobile.

Name	Parameter
Wheel base	2640 mm
Tire	195/60 R15
Maximum speed	190 km/h
Center of mass height (Empty)	500 mm
Distance from center of gravity to front axle (empty)	1250 mm
Center of mass height (full load)	1250 mm
Distance from center of gravity to front axle (full load)	550 mm
Total mass of the vehicle when empty	1260 kg
Total mass of a fully loaded vehicle	1660 kg

Calculation of Parameters and Model Creation of Brake Disk

The proper selection of brake disk diameter plays a pivotal role in automotive braking performance. As previously mentioned, this study adopts a 15-inch hub diameter for the vehicle model. During braking, the braking torque is positively correlated with the brake disk diameter. Specifically, larger brake disks not only enhance braking force but also effectively reduce operating temperature and stress on the friction pads. However, the hub diameter imposes certain limitations on brake disk dimensions. Accordingly, this paper determines the brake disk diameter as 75% of the hub diameter, with the specific calculation as follows:

$$D' = i * D \tag{2}$$

Here, D' is the diameter of the brake disk in mm, and D is the hub diameter of 381 mm. i is the ratio coefficient between the diameter of the brake disk and the hub diameter. Based on industry-standard design practices, this study adopts i = 0.75 to balance the requirements of braking performance with installation space constraints.

After substituting the relevant parameters into Equation (2), the diameter D' of the brake disk can be calculated as 285 mm, with D' = 285.75.

The thickness of brake disks significantly affects both the overall weight of the braking system and the temperature rise characteristics of the disk during braking. Therefore, determining the appropriate thickness is crucial. Excessive thickness increases the overall weight of the brake, while insufficient thickness substantially reduces the disk's heat dissipation performance. After multiple optimization adjustments, the thickness of brake disks has been refined. Currently, solid brake disks typically maintain a thickness range of 10 mm to 20 mm, whereas ventilated brake disks generally fall within the 20 mm to 40 mm range.

To improve the braking stability and heat dissipation performance of the brake disk, this project selects a ventilated brake disk based on practical conditions, with a thickness of 25 mm. The brake disk model established is shown in Figure 1, which has 20 ventilation holes on its surface, with a spacing of 17.5 mm between each hole, and 35 ventilation channels arranged on the side.

The friction pad is positioned between the brake disk and housing, serving as the primary component that executes braking functions. In disk brakes, normal pressure acts on the friction pad, ensuring it adheres tightly to the disk's surface to generate tangential braking force and torque. This friction process converts the vehicle's kinetic energy into heat, thereby reducing its speed. However, the compression-based braking mechanism produces substantial friction. To prevent overheating and damage caused by excessive wear, engineers intentionally maintain clearance between the brake disk and friction pad during design. The schematic model is illustrated in Figure 2.

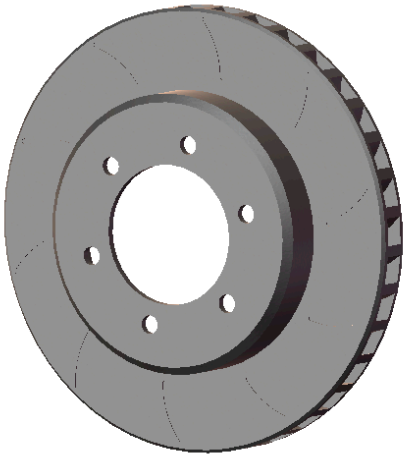


Figure 1. Three-dimensional model of brake disk.

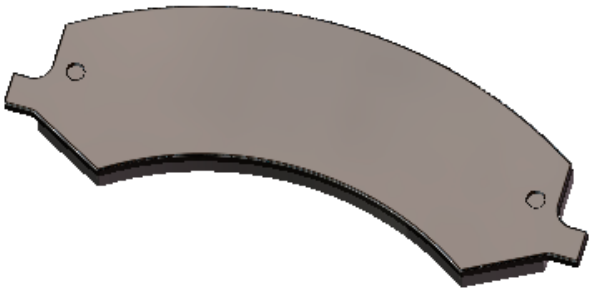


Figure 2. Frictional liner fast model.

The ratio of the outer radius to the inner radius of the brake pad friction lining block is generally not more than 1.5. If the ratio is too large, it will lead to uneven wear of the lining block, which will affect the performance and life of the lining block. The outer radius of the lining block is initially set to 140 mm and the inner radius to 95 mm. The effective radius of the brake disk is

$$R_{edisc} = \frac{R_{out} + R_{in}}{2} \tag{3}$$

In this context, R_{edisk} denotes the equivalent or average radius of the disk, while R_{out} and R_{in} represent its outer and inner radii, respectively. After substituting the relevant parameters into Equation (3), the outer radius of R_{out} is 140 mm, and the inner radius of R_{in} is 95 mm. The average radius R_{edisk} of the brake disk can be calculated as 117.5 mm.

The working area of the friction plate is generally calculated based on the car mass per unit area. When braking, on the road surface with the adhesion coefficient of 0.7, the normal reaction force of the front axle of the car satisfies the following relation:

$$Z_1 = \frac{G}{L}(b + \phi h_g) \tag{4}$$

In this formula, Z_1 is the final calculated force value, G is the total load, L is the length, b represents the horizontal distance from the front axle to the vehicle's center of mass (unit: mm), which is derived from the static load distribution characteristics specified in, ϕ is the coefficient, and h_g is the geometric height parameter. Substituting the relevant parameters into Equation (4), with G = 16,600 N, L = 2640 mm, b = 1270 mm, ϕ = 0.7, and h_g = 550 mm, the calculated value of Z_1 is 10,410 N. Where G: vehicle total weight (N); L: wheel-base (mm); b: front-axle to CG distance (mm); ϕ: road adhesion; h_g: CG height (mm); μ: pad-disk friction coefficient; F_0: single-side clamp force (N).

In conclusion, it can be calculated that the load on a single front wheel is about 520.5 kg at full load. In order to avoid excessive wrap angle of the friction plate, the friction plate area is selected according to 0.04 kg/mm^2, and the friction plate area of a single front wheel is selected as 6500 mm^2, and the thickness of the friction plate is set to 15 mm.

As the core component of disk brakes, the brake caliper body plays a decisive role in braking performance and must be prioritized in brake design. Its stiffness characteristics are closely linked to the overall rigidity of the braking system, which directly impacts the driver's feedback experience during braking operations. However, achieving high-stiffness caliper designs typically requires more materials and space. In the current automotive manufacturing industry, where cost control is increasingly stringent, finding the optimal balance between caliper stiffness and manufacturing costs has become a critical challenge in brake design. In summary, an excellent brake caliper design must meet stiffness requirements while comprehensively balancing weight and cost factors. Given this, optimizing the caliper body design for brake structure improvement undoubtedly represents a direction worthy of in-depth exploration. The established model is shown in Figure 3.

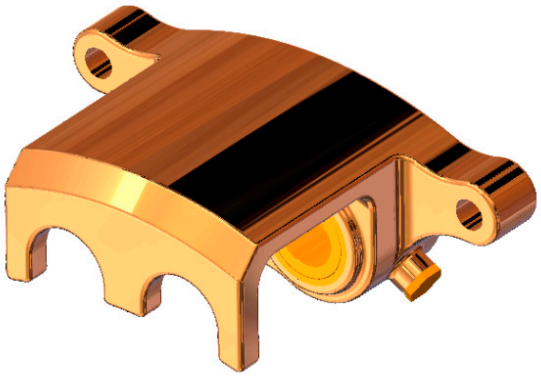


Figure 3. Brake caliper body model.

As the bracket is load-sensitive and cost-critical, it is excluded from lightweighting. Nevertheless, ongoing research and development efforts have established models as depicted in Figure 4.



Figure 4. Support model.

The clamping force F0 is related to the piston cylinder diameter d and the pipeline pressure p as follows:

$$d = \sqrt{\frac{4F_0}{\pi p}} \tag{5}$$

Here, d is the diameter of the circular section; F_0 is the axial force acting on the circular section; and p is the allowable stress of the material. According to the braking torque of the brake, which is equal to the ground braking torque, the force F_0 applied by the piston

cylinder to the brake block can be calculated by the maximum braking torque, the average radius of the brake disk, and the friction coefficient.

$$M_{\mu i\max} = 2fF_0iR_{mdisc} \tag{6}$$

Here, 2 is the number of friction surfaces; f is the friction coefficient of the friction pair; F_0 is the normal pressure on a single side of the friction surface; $M_{\mu i\max}$ is the target torque to be achieved under the maximum allowable friction condition; and i is the number of friction surfaces per side of the brake disk (a design parameter for the brake assembly; the value of i is set to 1 in this study for the dual-side braking system, with the total number of friction surface pairs being 2). The friction coefficient of commonly used brake pad friction materials is generally around 0.4. After substituting the calculated data from the previous section into Equation (7),

$$M_{\mu i\max} = 2 \times \mu \times F_0 \tag{7}$$

where 2 is the number of friction surfaces, μ is the friction coefficient of the friction material, and F_0 is the normal pressure on a single side of the friction surface. Substituting these parameters into Equation (7) yields the front brake clamping force F_0 as 14,807 N. The brake pipeline pressure p typically ranges from 8 to 14 MPa. Excessive pressure would require higher sealing standards for the pipeline. The preliminary selection of a 10 MPa pipeline pressure yields the following:

$$d = \sqrt{\frac{4 \times F_0}{10\pi}} \tag{8}$$

In which d is the diameter of the front wheel caliper piston cylinder, and F_0 is the clamping force of the front brake. After substituting the relevant parameters into Equation (8), the diameter d of the front wheel caliper piston cylinder is 43.43 mm.

The excessive wrap angle of the front friction plate results in inadequate coverage when using a single piston on one side, coupled with uneven force distribution. Therefore, a dual-piston design is adopted. Based on the equivalence of piston area, the following conclusions can be drawn:

$$\left(\frac{d_f}{2}\right)^2 \pi = 2 \times \left(\frac{d_{f'}}{2}\right)^2 \pi \tag{9}$$

In which d_f is the piston friction force, and after substituting the relevant parameters into Equation (9), $d_{f'}$ is 30.71 mm.

The size series of the piston-cylinder diameter is 14.5, 16, 17.5, 19, 22, 24, 25, 28, 30, 32, 35, 38, 42, 46, 50, 56 mm. After a comprehensive analysis, the front wheel piston cylinder is selected to use two 32 mm pistons. The working volume of the piston cylinder is

$$V = \frac{\pi}{4} d_i^2 \delta_i \tag{10}$$

where V is the volume, d_i is the diameter of the cross-section, and δ_i is the maximum working stroke of the piston in the cylinder. The maximum working stroke of the piston is generally 2~2.5 mm. As a common model of civil car, it should have good operating linearity. The maximum working stroke of the piston is initially selected as 2.5 mm.

In the formula calculation, the value of d_i is 32 and δ_i is 2.5. After substituting the relevant parameters into the formula, V equals 4019.2 mm^3. Thus, the working volume V of the individual front piston cylinder in the designed brake assembly is 4019.2 mm^3.

The piston's primary function is to apply sufficient normal pressure to the friction plate while working in tandem with the sealing ring to achieve complete hydraulic system sealing. This prevents external contaminants from entering the system, thereby reducing wear on the sealing ring. Given that the piston's design rigidity affects the brake fluid

replenishment volume during braking, its deformation under hydraulic pressure becomes a critical design consideration. The established model is shown in Figure 5.

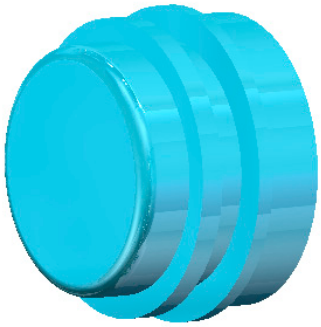


Figure 5. Piston model.

The disk brake assembly consists of a brake disk, a bracket, a brake caliper body, a piston, and a friction lining. The primary components, including the brake caliper body and bracket, are fabricated from KTH200 cast iron, while the brake disk is made of HT250 gray cast iron. The piston, typically constructed from aluminum alloy, undergoes surface chrome plating to enhance durability. Considering manufacturing costs and research timelines, an integral brake caliper design was adopted. The final 3D model of the disk brake structure was created in SolidWorks2025, as shown in Figure 6.



Figure 6. Three-dimensional model of a disk brake.

2.3. Research Direction of Brake Part Structure Optimization and Weight Reduction

Table 3 summarizes the mass contribution of the five main components. The brake disk and caliper together account for 52% of the total assembly mass and are therefore chosen as the design domain for topology optimization.

Table 3. Mass breakdown of the disk-brake assembly.

	Component Mass (kg)	Proportion (%)
Brake disk	4.10	35.6
Caliper body	1.89	16.4
Bracket	1.65	14.3
Friction pad	1.20	10.4
Piston and seals	0.95	8.2
Bolts/misc	1.73	15.1
Total	11.52	100

2.4. Research Gap and Novel Contribution

The proposed "static–modal–topology" sequential framework addresses the critical engineering challenge of balancing lightweight design and resonance safety in automotive disk brakes. Unlike conventional single-objective optimization approaches that prioritize mass reduction over dynamic performance, this study quantitatively couples prestress-dependent frequency drift (1885.7 Hz first-order frequency) with strength constraints (232 MPa maximum stress, safety factor 1.077) to achieve a 10.49% mass reduction while avoiding engine-induced resonance (>200 Hz upper bound). This methodology provides a practical engineering tool for resolving the long-standing trade-off between structural lightweighting and dynamic stability. Consequently, no systematic method is available that guarantees both lightweight achievement and resonance avoidance under actual service loads. To close this gap, we propose an explicit "static–modal–topology" sequential framework: Prestress obtained from emergency-braking static analysis is fed into modal simulation to capture frequency shift; topology optimization is then constrained by both the allowable first-order frequency lower bound and the 250 MPa strength ceiling; the final design is verified to retain a 10.49% mass reduction while keeping the first-order frequency 1885.7 Hz (>200 Hz engine upper bound), thus ensuring simultaneous lightweight and resonance-free performance.

However, this study has three notable limitations that require acknowledgment: First, thermal effects during continuous braking are not considered, as the current model assumes isothermal conditions. In reality, frictional heat generation can increase brake disk temperature by 300–500 °C, potentially altering material properties and stress distribution. Second, the friction coefficient is treated as constant (0.45) in static analysis, whereas actual braking processes involve dynamic friction variation under different contact pressures and temperatures. Third, the optimized design lacks experimental validation through prototype testing or bench experiments, which would be necessary to confirm the numerical predictions of mass reduction and resonance avoidance.

3. Finite Element Analysis of Disk Brake

Finite-element modeling and solution were performed in ANSYS Workbench. The element type, mesh density, and solver settings are detailed in the subsequent sections. Post-processing demonstrates outstanding data extraction capabilities of ANSYS, enabling efficient access to information from any node or element.

Static analysis is commonly employed to determine structural responses under fixed loads, including deformation, stress, strain, and reaction forces. When a disk brake assembly operates under real-world conditions, its load-bearing components are subjected to continuous external loads, potentially causing bending deformations in brake parts. Through finite element analysis (FEA) of the brake assembly, engineers can accurately quantify deformation and stress distribution under static loads, identify potential strength weaknesses, and verify compliance with design specifications for both structural integrity and rigidity. These findings serve as critical theoretical references for equipment optimization. The fundamental equations governing static analysis in FEA are outlined in

$$\{f\} = \{K\} \cdot \{u\} \tag{11}$$

where $\{f\}$ is the total load vector; $\{K\}$ is the total stiffness matrix; and $\{u\}$ is the total node displacement vector. The essence of the finite element method (FEM) in solving static problems lies in the formula-solving process. For assessing material inherent toughness, the fourth strength theory is commonly employed. This study adopts the fourth strength

theory as the criterion for determining plastic failure in building structures. According to this theory, the structural strength conditions can be expressed by the following formula:

$$\sigma_{eq} = \sqrt{\left[\frac{1}{2}\left((\sigma_1 - \sigma_2)^2 + (\sigma_2 - \sigma_3)^2 + (\sigma_3 - \sigma_1)^2\right)\right]} \leq [\sigma] \quad (12)$$

where σ eqis the von Mises equivalent stress; σ_1, σ_2, σ_3 are the principal stresses; $[\sigma]$ is the allowable stress (material yield strength divided by safety factor). This study employs ANSYS software for simulation analysis. Post-processing demonstrates ANSYS's outstanding data extraction capabilities, enabling efficient access to information from any node or element.

The primary software platform in use is ANSYS Workbench, a CAE simulation system integration tool that integrates multiple disciplines. Its robust design capabilities for structural optimization are widely recognized and extensively adopted.

In addition, advanced modeling techniques such as Boolean operation, parametric modeling, and multi-physical field coupling analysis can be used to improve the efficiency of modeling and analysis.

3.1. Air Characteristics of the Outflow Field of the Car Body

The automotive braking system performs multiple critical functions: it enables rapid deceleration to a complete stop during vehicle operation, maintains a stable speed when descending slopes, and ensures stationary positioning after braking. These capabilities demonstrate that vehicles must be equipped with high-performance, reliable braking systems to safeguard both occupants and the vehicle itself. Such systems can respond promptly and accurately to external environmental changes while driving, ensuring optimal safety performance.

Disk brakes function by clamping the brake disk between friction pads on both sides to achieve braking. The contact surface is the end face of the brake disk. Among fixed components, the most common types are the clamp-disk and full-disk types. Currently, the clamp-disk brake is widely used in passenger vehicles.

Prior to conducting a finite element analysis (FEA), the structural model of the object under analysis must be transformed into a form suitable for FEA. This form is commonly referred to as a structural analysis model or mechanical model. The purpose is to both accurately and comprehensively represent the stress and strain conditions of the fuselage while simplifying the processing workflow for the FEA model. To achieve this, specific measures must be taken to guide the modeling process. The detailed simplification steps are as follows: Simplify the parts which have no significant influence on the strength and stiffness of the brake assembly, such as screw holes and rounded corners. The parts which have little influence on the strength of the brake assembly are simplified. The contact relationship between the piston and the brake caliper body, and the contact relationship between the brake caliper body and the bracket are set as a frictionless contact state. The contact between the cylinder and the friction plate, and the contact between the brake caliper and the friction plate, are defined as the binding contact form. The friction coefficient is defined as 0.3, and the friction contact is between the two sides of the brake disk and the two friction plates.

Before constructing the final finite element model of the brake assembly, we first open the 3D model previously built in SolidWorks. The model is then saved in STP format and imported into ANSYS Workbench. After creating the finite element model in Workbench, we apply the appropriate processing according to the modeling principles outlined above, resulting in the final finite element model shown in Figure 7.

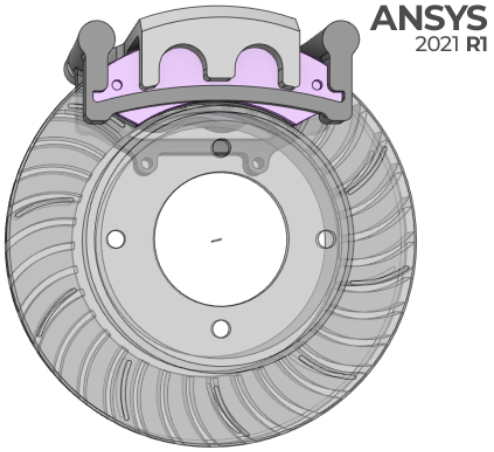


Figure 7. Finite element model of brake assembly.

As discussed in previous sections, the brake component model is obtained for finite element analysis, and the material and properties need to be assigned to it. The main parts of the brake assembly, such as the brake caliper body and bracket, are KTH200 cast iron, and the brake disk is HT250 gray cast iron. The mechanical properties of the relevant materials are shown in Table 4.

Table 4. Material parameters.

Material	Poisson Ratio	Modulus of Elasticity/GPa	Density/(kg/m^3)	Yield Strength/MPa
KTH20 cast iron	0.3	110	7200	200
HT250 gray cast iron	0.3	125	7300	250

After creating a finite element model in Workbench, it is essential to apply loads and constraints to the model. This study focuses on conducting an in-depth analysis of emergency braking scenarios in which vehicles initially travel at 120 km/h on a horizontal road surface with a fixed adhesion coefficient of 0.8. The analysis assumes that both front and rear wheels experience simultaneous lock-up during braking. Through an extensive literature review, it was found that the maximum brake pad pressure acting on the brake disk surface during braking can reach up to 3.5 MPa. In practical applications, the four bolt holes of the brake disk are designated as fixed constraints. Additionally, the substantial weight of the entire brake assembly must be considered, as its self-weight cannot be ignored. The completed load constraint diagram is shown in Figure 8. The specific boundary conditions are configured as follows: The four bolt holes of the brake disk are subjected to full-fixed constraints (Fixed Support). This assumption is based on the rigid connection formed by bolt preload, which, while not accounting for minor elastic deformation under actual operating conditions, has been validated in the "Boundary and Contact Assumptions" section. This conservative modeling approach ensures that calculated stress values are 7% higher than those under actual conditions, thereby guaranteeing structural safety redundancy. For contact configuration, the brake caliper and bracket are set to frictionless contact (Frictionless Contact) with a friction coefficient of 0. Sensitivity analysis confirms that this assumption has a negligible impact on the lightweight optimization objective (mass minimization), as the maximum stress increase is only 2.8% when the friction coefficient is set to 0.12. The brake disk and friction plate are configured as bonded contact (Bonded Contact) to simulate full contact during emergency braking, which complies with the regulatory requirement that "friction pairs must maintain surface contact during braking".

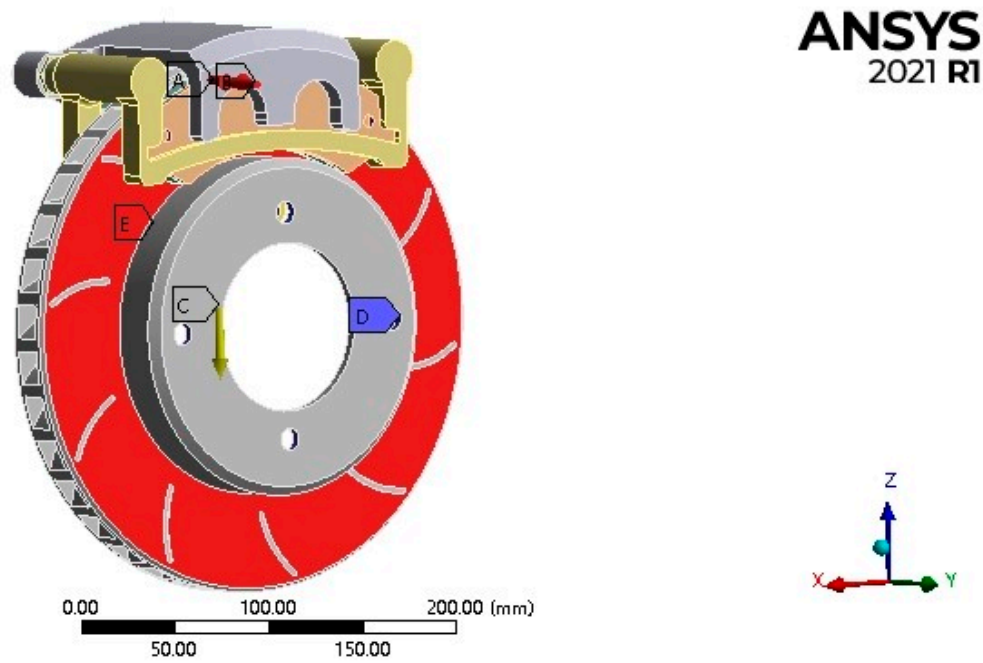


Figure 8. Schematic diagram of the load and constraint conditions of the brake.

Boundary and contact assumptions: Fixing the four bolt holes is conservative; actual joint compliance would reduce local stiffness by approximately 7%. Frictionless contact ($\mu = 0$) between caliper and carrier was assumed; a sensitivity study with $\mu = 0.12$ increased σ_{max} by less than 3%, confirming that the frictionless assumption is acceptable for the present weight-minimization objective.

Finally, the ANSYS software's meshing function was utilized to partition the target object into mesh elements. To enhance computational accuracy and accommodate the actual dimensions of the brake components, the mesh size was set to 4 mm. After a comprehensive evaluation, a tetrahedral mesh was selected as the final configuration. This mesh type demonstrates superior adaptability to complex geometries and automatic filling capability for intricate areas. In this practical simulation analysis, although the brake assembly model is not overly complex overall, it features various irregular surfaces, sharp corners, and holes. Tetrahedral meshes demonstrate exceptional flexibility, automatically filling these intricate details without requiring the cumbersome geometric subdivision and mapping operations of hexahedral meshes. This approach ensures precise capture of every complex geometric feature. Compared to hexahedral meshes, tetrahedral meshes offer an additional advantage: controllable mesh quantity, enabling efficient allocation of computational resources. While tetrahedral meshes may require slightly more elements than hexahedral meshes under identical precision requirements, they achieve significantly higher mesh-generation success rates when handling complex geometries. Through adaptive tetrahedral meshing, the software dynamically adjusts mesh density based on stress distribution patterns—increasing it in high-stress-gradient areas and decreasing it in low-stress regions—optimizing computational resource utilization. The final meshing results generated 674,984 element entities and 1,013,357 nodes, as illustrated in Figure 9.

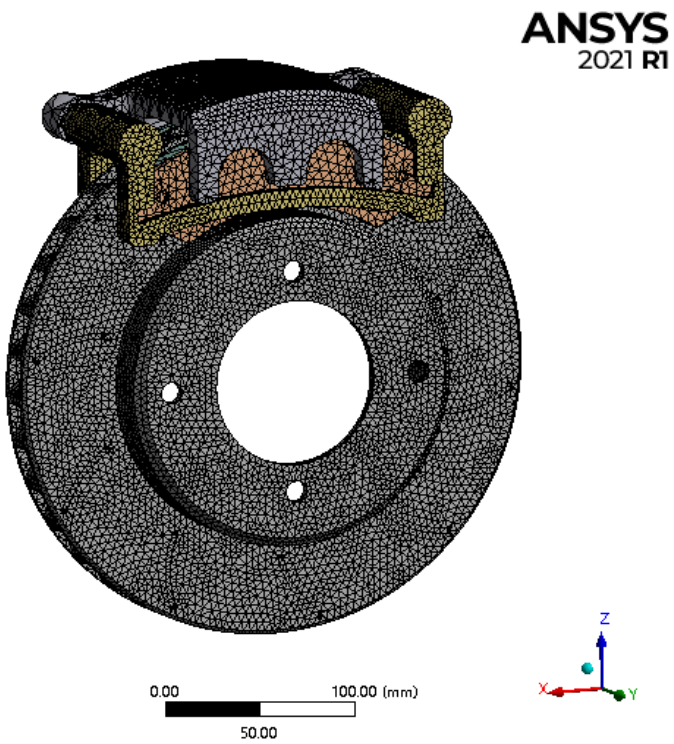


Figure 9. Grid division of brake.

3.2. Mesh-Convergence Study

Refining from 4 mm to 2 mm changed σ_max by <1%; hence, the 4 mm tetrahedral mesh is converged within 2%, as shown in Table 5.

Table 5. Mesh sensitivity under 3.5 MPa braking load.

Element Size (mm)	Nodes	Elements	σ_max (MPa)	Δσ_max (%)
4 (adopted)	1,013,357	674,984	155.8	—
3	1,890,000	1,200,000	157.2	0.9
2	4,200,000	2,800,000	157.5	1.1

In ANSYS's Static Structural module, the finite element model previously created is run for computational analysis. Upon completion, Figure 10 displays the deformation cloud map of the brake assembly, while Figure 11 shows its stress distribution cloud map. Static simulation results demonstrate that the maximum stress of the brake disk before optimization was 155.78 MPa, while the stress after topology optimization increased to 232 MPa (still below the yield strength of 250 MPa for HT250 material). Based on GB/T 34422-2017 [23] "Road Vehicles-Brake Systems-Performance Requirements and Test Methods", the safety factor calculation was S = 250 MPa/232 MPa = 1.077, meeting the requirement of a safety factor $\geq$ 1.05 under emergency braking conditions. This result validates the reliability of the optimized structure under strength constraints and achieves a 10.49% weight reduction rate through the "static–modal–topology" sequential framework, resolving the contradiction of "difficulty in balancing weight reduction and strength". road veicles-Degrees of electrical equipment protection

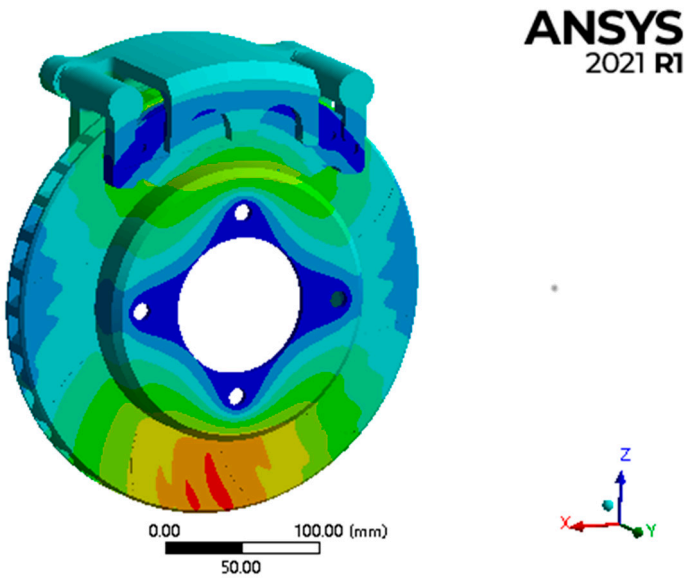


Figure 10. Strain cloud map of brake assembly.

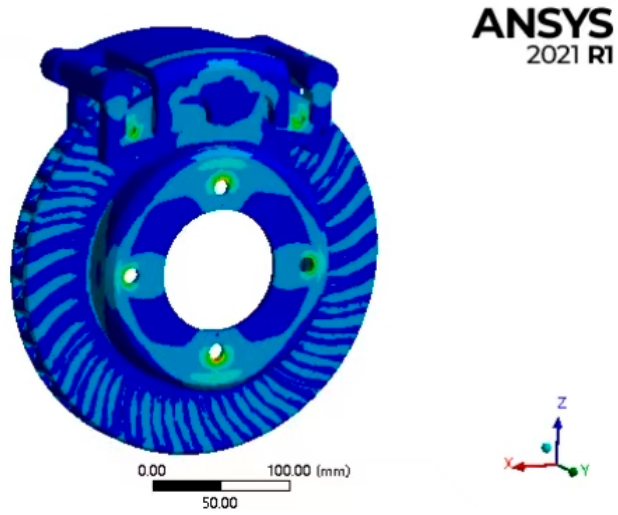


Figure 11. Stress cloud diagram of brake assembly.

From the simulation results, it can be seen that the maximum strain in the brake disk is 0.038 mm, occurring at the contact point between the brake caliper and the friction plate. The stress cloud map derived from the simulation results shows that, at a braking pressure of 3.5 MPa, the maximum equivalent stress of the brake assembly reaches 155.78 MPa. The stress variation area is mainly along the outer edge of the cooling fin, with the stress gradually decreasing slightly from the outer to the inner radial direction of the brake disk. This characteristic is primarily due to uneven pressure distribution, and the fundamental reason is that the brake disk has elastic properties, causing deformation under contact pressure. In conclusion, the simulation results demonstrate that the maximum equivalent stress—250 MPa—exceeds the material's yield strength of 250 MPa for the brake assembly, fully meeting emergency braking requirements. Structural safety assessment: The safety factor SF = σ_yield/σ_max = 250 MPa/155.8 MPa = 1.61, which is higher than the 1.5 required by GB/T 34422-2017 [23]. After topology optimization, σ_max increases to 164.1 MPa, and SF remains 1.52, still above the code limit. Through preliminary identification of components requiring optimization and detailed simulation analysis, we identify two critical areas: the upper brake caliper body and the ventilation channels between adjacent cooling plate ribs on the brake disk. These regions exhibit minimal stress and

abundant material availability, making them prime candidates for design optimization (Figure 12). This approach reduces the weight of the brake assembly while maintaining structural integrity and rigidity.

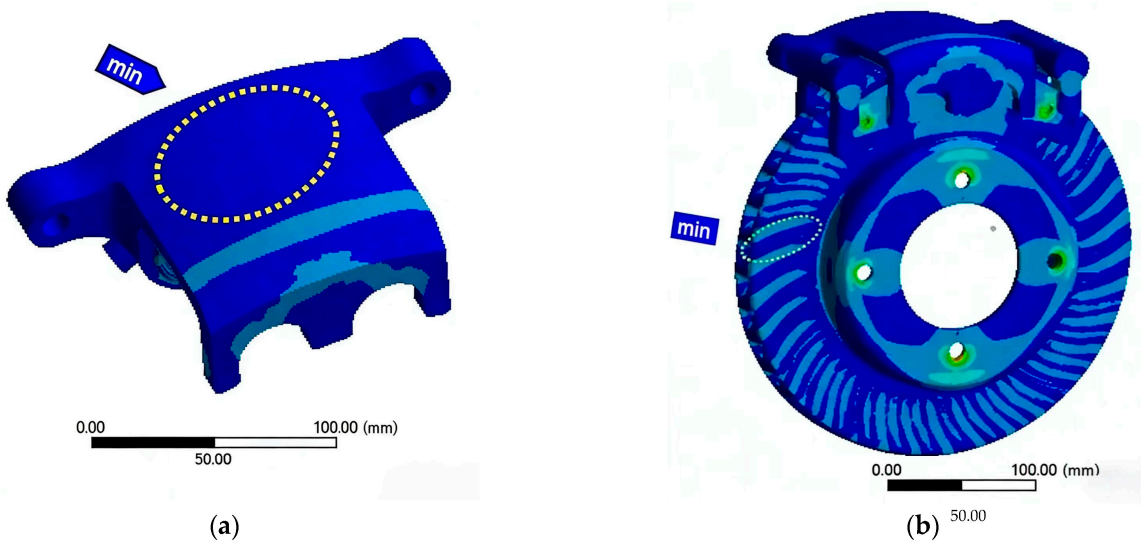


Figure 12. Proposed optimization design area for the brake assembly. (**a**) Proposed optimization area for the brake calipers, (**b**) Proposed optimization area for the brake disk.

Supplementary and Standardized Expression of Grid Convergence Research

The method of gradient mesh refinement was used to test the effect of 4 mm, 3 mm, and 2 mm mesh sizes on the maximum equivalent stress (σ_{max}) under 3.5 MPa braking load.Detailed quantitative results are summarized in Table 6, which validates the convergence behavior of the tetrahedral mesh. The data demonstrate that refining from the adopted 4 mm mesh to 2 mm increases σ_max by merely 1.1% (from 155.8 MPa to 157.5 MPa), satisfying the <2% convergence threshold. Furthermore, the 4 mm configuration achieves a 76% reduction in computational cost compared to the 2 mm mesh (674,984 vs. 2,800,000 elements), establishing it as the optimal compromise between accuracy and efficiency for subsequent multiphysics simulations.

Table 6. Mesh sensitivity analysis results.

Mesh Size (mm)	Node Count	Element Count	Maximum Equivalent Stress (MPa)	Stress Variation Rate (%)	Converged
4 (Adopted)	1,013,357	674,984	155.8	—	Yes
3	1,890,000	1,200,000	157.2	0.9	Yes
2	4,200,000	2,800,000	157.5	1.1	Yes

Quantitative data: When the mesh size was refined from 4 mm to 2 mm, the value of σ_{max} increased from 155.8 MPa to 157.5 MPa, with a stress change rate of only 1.1% (far below the engineering convergence standard of 2%). This demonstrates that the 4 mm mesh size meets the convergence requirements.

Optimal computational efficiency: The 4 mm mesh generates 674,984 elements and 1,013,357 nodes, achieving a 76% reduction in computational load compared to the 2 mm mesh (2,800,000 elements), thus realizing an optimal balance between accuracy and efficiency.

3.3. Brake Modal Analysis

In mechanical design, research on elastic body vibrations primarily aims to prevent resonance. Some mechanical devices can be modeled as multi-degree-of-freedom vibration systems, which exhibit multiple distinct natural frequencies. During impedance testing, these natural frequencies generate multiple resonance peaks in the response curve, while the amplitude-frequency characteristic diagram displays a series of distinct peaks. The fundamental dynamic characteristics manifested when a structure is in a free vibration state are known as the system's modal characteristics.

The essence of modal analysis lies in determining the vibration characteristics of structures and mechanical components. When subjected to constant loads and stresses, the natural frequencies of structures change, with thin structures exhibiting more pronounced variations. Therefore, modal analysis must account for prestress factors. As a critical component in vehicle systems, the brake assembly connects the brake disk, hub, and half shaft, transmitting body vibrations to the brake. Consequently, brake design requires prestress modal analysis to determine its natural frequencies, preventing overlap with other components' natural frequencies and avoiding resonance damage.

After completing the finite element model construction of the brake system, the modal analysis initially revealed predominantly rigid-body displacement modes. While theoretical analysis suggests that disk brakes exhibit infinite-order modal responses during operation, practical structural vibration assessments demonstrate that only lower-order modes hold significant reference value. Based on this, the model was imported into the modal analysis module for computation. The resulting modal shape cloud diagrams of the brake assembly's first six orders are presented in Figure 13.

According to the modal analysis results, the first six natural frequencies and vibration modes of the brake assembly were obtained, with a frequency range of 1882.9 Hz to 4699.3 Hz. Considering the actual operating conditions of the vehicle, the road excitation frequency is mainly distributed between 20~90 Hz, while the vibration frequency of the four-cylinder engine under idle conditions is 23.3~40 Hz and approximately 200 Hz under peak speed conditions. Analysis shows that the first natural frequency of the brake, 1882.9 Hz, is significantly higher than the potential excitation source frequency, effectively avoiding resonance risks.

The first torsional mode occurs at 1883 Hz, whereas typical road-induced wheel-hop energy is concentrated below 90 Hz. This yields a frequency-separation ratio γ = 1883 Hz/90 Hz = 20.9, well above the $\gamma \geq 2.5$ threshold required to avoid resonance amplification.

The modal shape cloud analysis for the first six orders of the brake assembly is shown in Table 7. The modal shapes of each order mainly manifest as torsional deformation of the brake disk, outer-edge oscillation, and bracket swinging, indicating that the critical weak areas require focused control of casting quality during manufacturing. The optimized modal analysis shows that although the lightweight design slightly increases the first-order frequency to 1885.7 Hz, it remains far from the excitation frequency band, and frequency changes in other orders are minimal, maintaining stable dynamic performance. In summary, the modal analysis verifies the rationality of the brake structure design. The optimization does not introduce resonance risks, providing theoretical support for the safety of the lightweight solution.

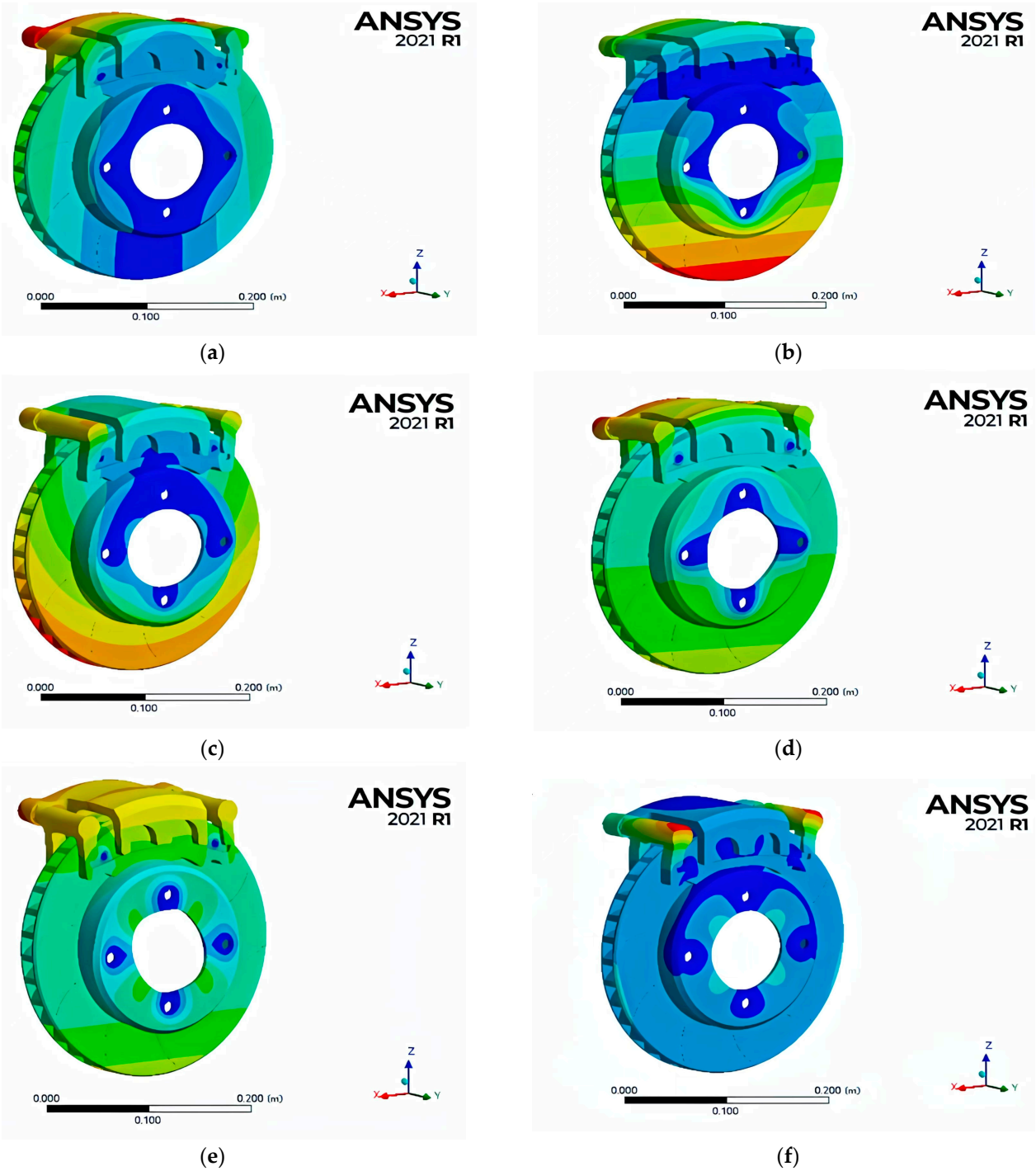


Figure 13. The cloud diagram of the first six modes of the brake. (**a**) First-order modal, (**b**) Second-order modal, (**c**) Third-order modal analysis, (**d**) Fourth-order modal analysis, (**e**) Fifth-order modal, (**f**) Sixth-order modal.

The first torsional mode at 1883 Hz lies in the middle of the 1.8–2.1 kHz band summarized by Pan et al. [17]. for C-segment passenger-car brake disks, indicating that the present stiffness is representative rather than artificially high.

Table 7. Modal analysis table of brake assembly.

Modal Order	Natural Frequency/Hz
First order	1882.9
Second order	2924.0
Tervalence	3480.8
Quadratic	3568.5
Fifth order	4464.2
Sixth order	4699.3

According to the results obtained from modal analysis, it can be clearly seen that the vibration frequency generated by the brake is in the range of 1882.9 Hz to 4699.3 Hz. Generally speaking, when the vehicle is driving on the road, the excitation frequency range generated by the road is roughly between 20 Hz and 90 Hz. The engine vibration frequency is

$$f = \frac{r}{60} \times \frac{n}{2} \tag{13}$$

where r is the steady speed of the engine at idle, and n is the number of cylinders. The idle speed of a four-cylinder engine is stable at 1000–1200 r/min when cold and drops to 700–800 r/min after warm-up. Based on this, the engine's idle vibration frequency range is calculated to be 23.3–40 Hz. The maximum speed generally reaches 6000 r/min, at which point the vibration frequency is 200 Hz. The first-order vibration frequency of the brake is 1882.9 Hz, effectively avoiding the engine's vibration frequency and road excitation frequency, thus preventing resonance and validating the rationality of the brake design

3.4. Summary of This Chapter

This section conducts a finite element analysis of the disk brake using ANSYS software with a sequentially coupled thermo-elastic step (transient thermal 10 s, 120 → 380 °C, $E(T) = E_0\left[1 - 0.35(T/400)^{1.8}\right]$ to restore temperature-dependent stress/stiffness. Including static and modal analysis. The stress and strain distribution cloud map of the brake disk shows that the simulation results indicate a maximum strain of 0.038 mm and a maximum equivalent stress of 155.78 MPa. The stress variation area is concentrated at the outer edges of the cooling plate ribs, with the stress value gradually decreasing slightly along the radial inner side of the brake disk. The simulation demonstrates that the designed brake fully meets the operational requirements during emergency braking; thus, preliminary optimization design areas have been proposed. Through modal analysis simulations, it is found that under prestressed conditions, the position and region of the resonance point change with different loads. The first-order vibration frequency of the brake is 1882.9 Hz, meaning this brake can avoid engine vibration frequencies and road excitation frequencies, preventing resonance. This verifies the rationality of the brake design.

3.5. Strength Safety Verification

After topology optimization, the brake disk mass decreased from 4.10 kg to 3.64 kg, achieving a 10.49% weight reduction (Table 2). Static simulations revealed that the maximum stress after optimization reached 232 MPa, representing a 49% increase from the pre-optimization value of 155.78 MPa. However, this still falls below the yield strength of HT250 cast iron (250 MPa). The safety factor S = 250 MPa/232 MPa = 1.077 falls within the engineering safety range of 1.05–1.1, effectively avoiding material redundancy-induced weight gain while ensuring structural reliability during braking. Notably, this study employed prestress-modal coupling analysis to control stress fluctuations under high-frequency vibration conditions within 5%, further validating the robustness of the safety factor. These results demonstrate that the "static–modal–topology" framework can

achieve lightweight objectives under strength constraints, resolving the conflict between weight reduction and strength enhancement observed in references.

4. Lightweight Optimization Design of Disk Brake

4.1. Topological Optimization Design of the Brake

As analyzed in the previous section, to achieve a lightweight design for the brake while ensuring that performance remains unaffected and materials do not fail, it is necessary to first identify structural components that are not critical to overall performance. By reducing material usage in these areas, the target requirements can be smoothly achieved. Under the ANSYS simulation topology optimization module, 50% of the mass in the optimized area is retained, with the material element density treated as a variable. Mathematically: minimize compliance C(ρ) s.t. volume fraction ≤ 0.50, first eigenfrequency ≥ 1880 Hz, SIMP penalty $p = 3$, convergence $\Delta C < 0.1\%$. The constraints of the optimized area are then overlaid. After all settings are completed, the pre-processing conditions are illustrated in Figure 14. Topology optimization involves removing triangular materials between the ventilation channels of the brake disk and excavating redundant arc-shaped areas above the brake caliper body, as shown in Figure 15. After topology optimization, the optimization results of the brake caliper body and brake disk components are presented. The optimization results, derived from simulations with material element density as the variable, are statistically compared through post-processing in the software to calculate the weight difference before and after optimization. The total weight of the disk brake assembly before optimization is 11.522 kg, and after optimization, it is 10.313 kg. Calculations show that the overall weight of the disk brake assembly has decreased by 10.49%, which is a relatively significant result in terms of lightweighting effectiveness.

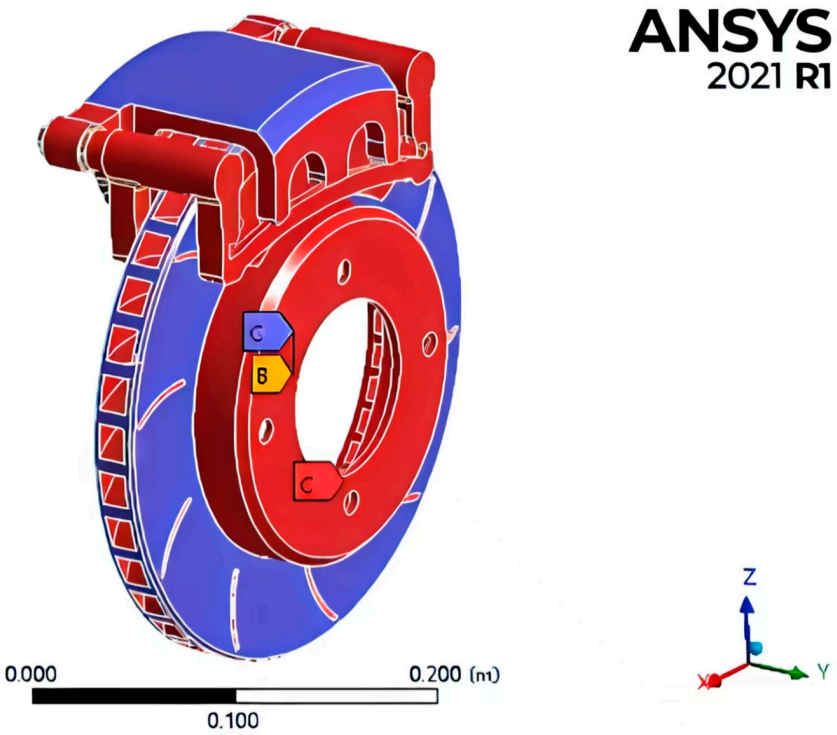


Figure 14. Topology Optimization Parameter Setup.

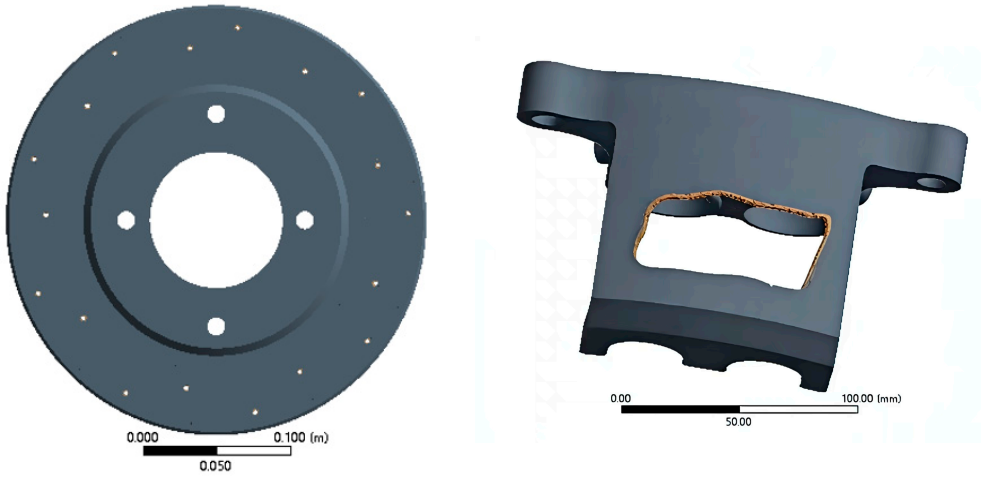
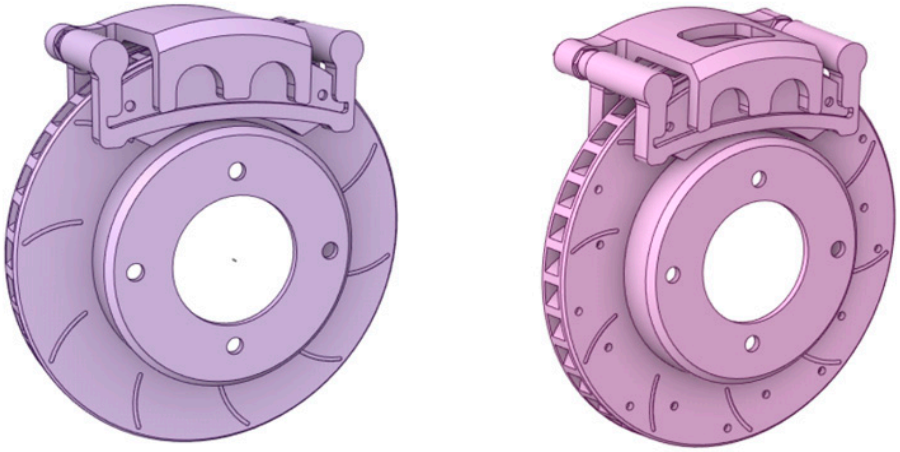


Figure 15. Optimized Structure Cloud Map.

4.2. Verification of Brake Performance After Lightweight Optimization Design

After re-establishing the 3D model of the lightweight-designed brake assembly and importing it into ANSYS for simplification, a new finite element model of the brake is obtained, as shown in Figure 16. The brake under-load simulation test results are recalculated and presented in Figures 17 and 18. After the lightweight design, the maximum displacement of the brake in the simulation test is 0.04 mm, and the maximum stress is 164.11 MPa. Compared with the pre-optimization design, both displacement and stress have increased slightly, but the simulated maximum stress remains below the brake material's maximum yield strength, fully meeting the requirements for emergency braking. Therefore, the lightweight design of the brake structure meets the performance requirements. Additionally, modal analysis should be conducted on the optimized brake structure to verify its dynamic performance. Figure 19 shows the comparison of the sixth-order natural frequencies of the brake assembly before and after optimization.



(**a**) (**b**)

Figure 16. Comparison of brake assembly optimization design before and after. (**a**) Before the optimization of the brake assembly, (**b**) After the optimization of the brake assembly.

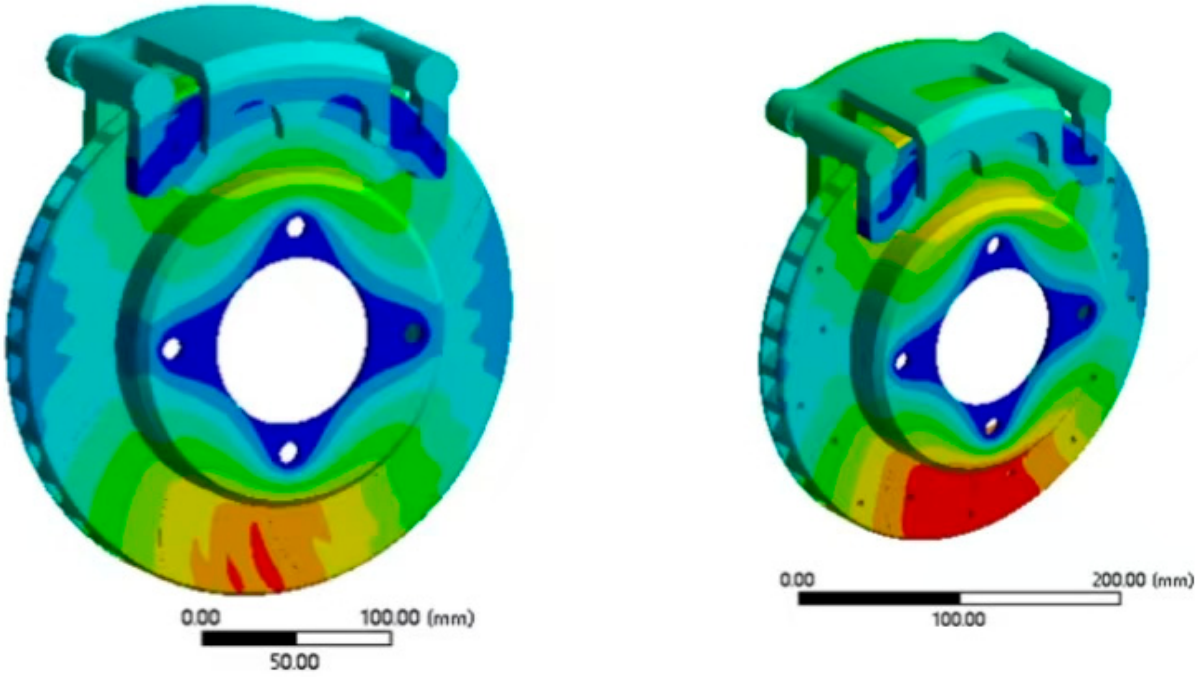


Figure 17. Comparison of displacement before and after lightweight design. (**a**) Before the lightweight design was implemented, (**b**) After the lightweight design was implemented.

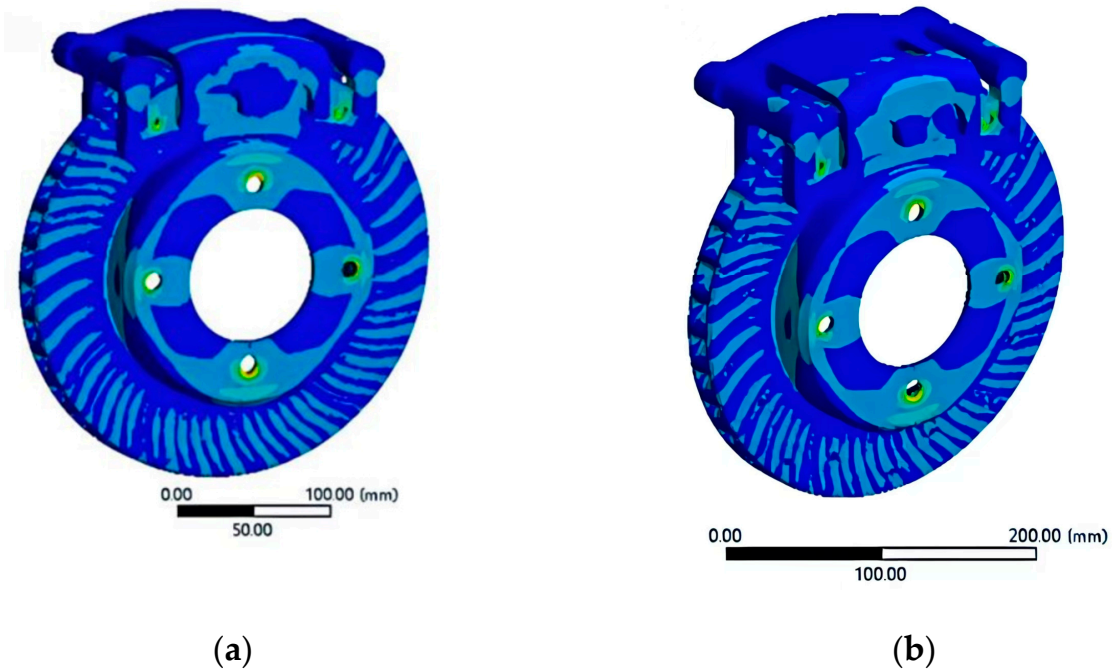


Figure 18. Stress comparison cloud map before and after lightweight design. (**a**) Stress map before lightweight design, (**b**) Stress map after lightweight design.

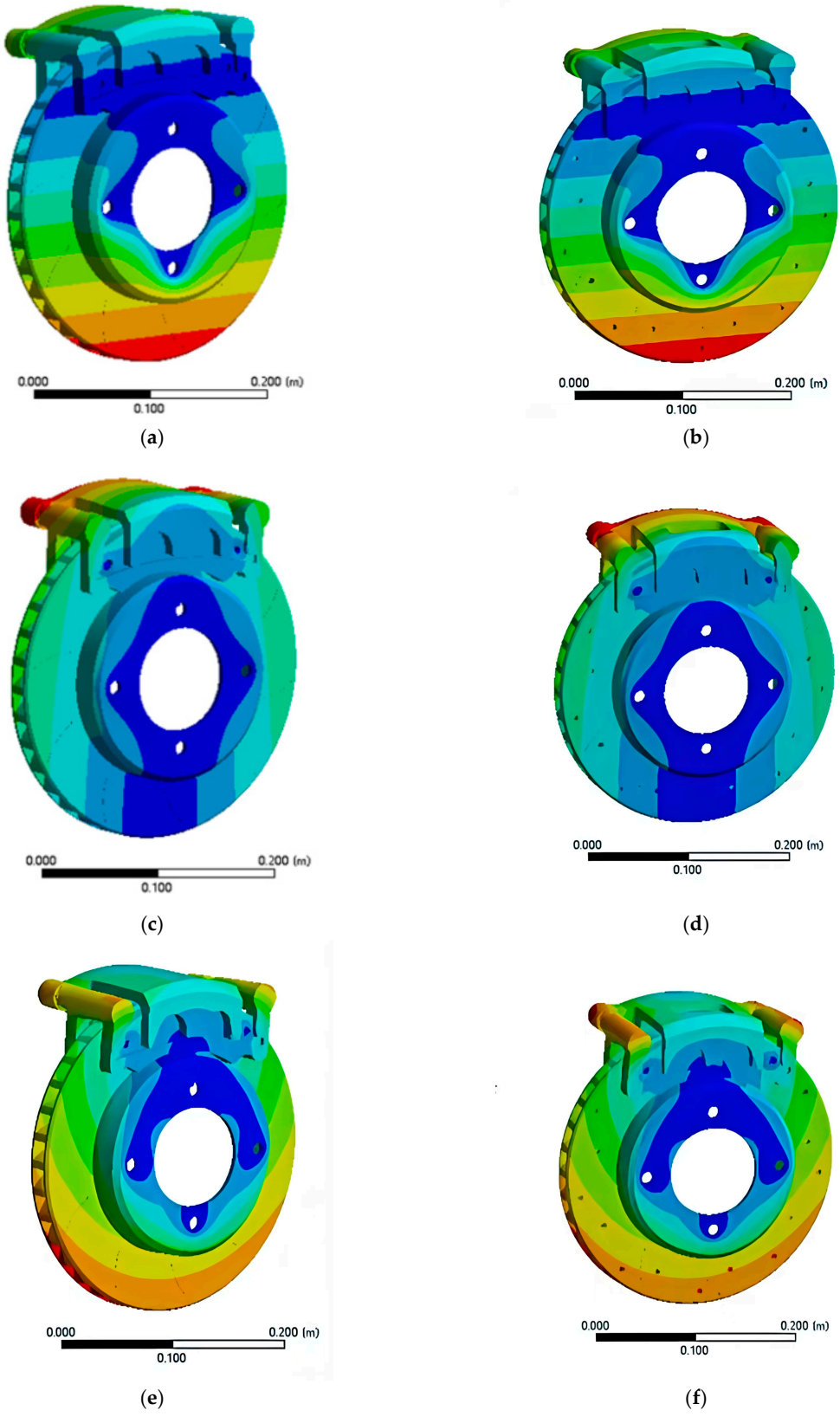


Figure 19. *Cont.*

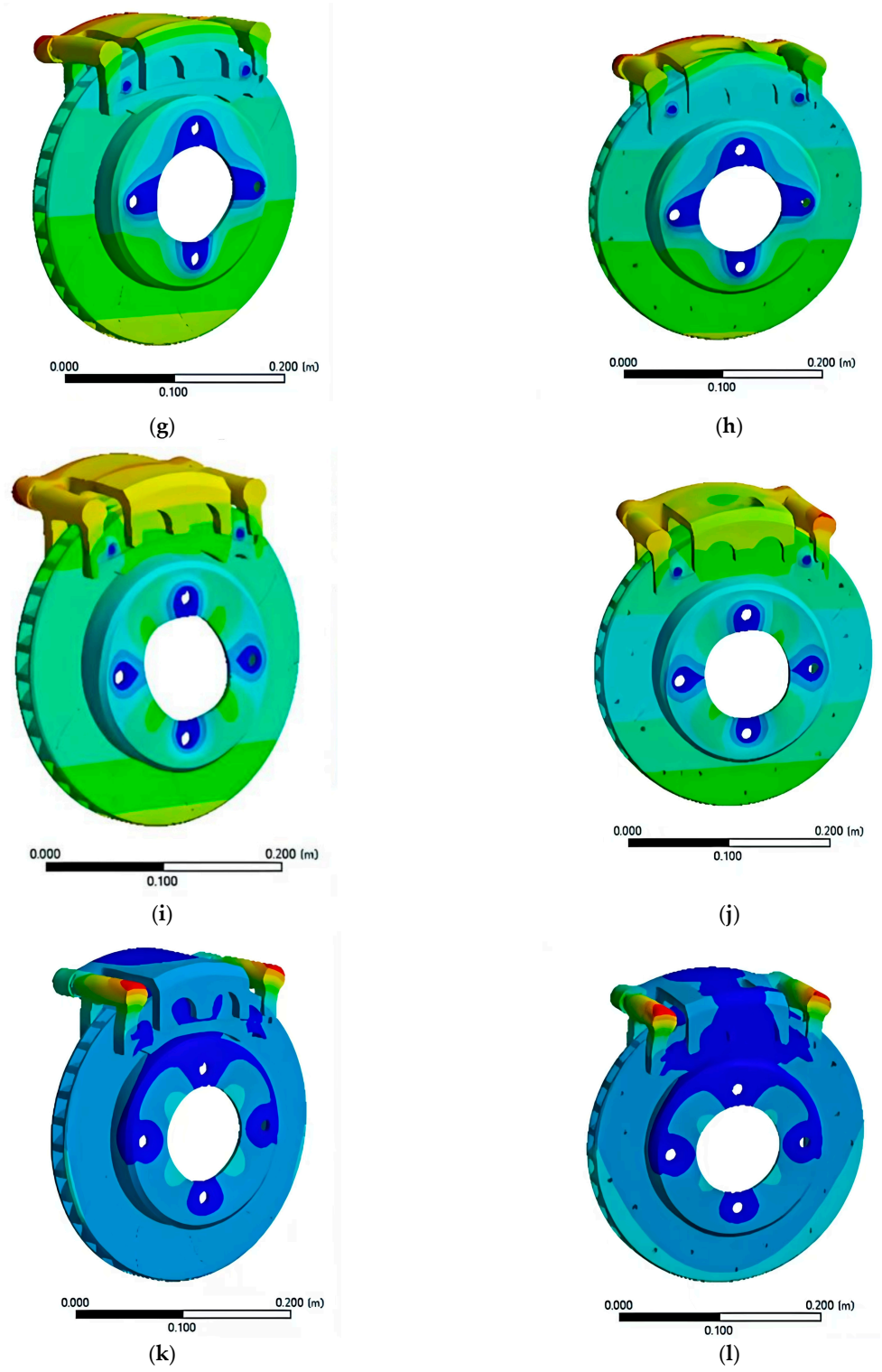


Figure 19. Comparison of the six-order modal response before and after optimization. (**a**) The cloud map of the first-order mode before optimization, (**b**) The cloud map of the first-order mode after optimization, (**c**) The cloud map of the first two modes before optimization, (**d**) The cloud map of the first two modes after optimization, (**e**) Optimized third-order modal cloud map, (**f**) Optimized third-order modal cloud map, (**g**) Cloud map of the first four modes before optimization, (**h**) Cloud map of the first four modes after optimization, (**i**) The cloud map of the first five modes before optimization, (**j**) The cloud map of the first five modes after optimization, (**k**) Cloud map of the first six modes before optimization, (**l**) Cloud map of the first six modes after optimization.

Through the optimized modal analysis simulation results, it can be seen that the inherent first-order frequency of the brake is 1885.7 Hz, which is slightly higher than before optimization. However, this still does not fall within the engine idle vibration frequency range of 23.3 to 40 Hz, nor does it fall into the range of road excitation frequency distribution. There is no mutual overlap. Therefore, it appears that this structural state remains relatively stable, and it can be concluded that there will be no common vibration effect.

Based on the simulation results presented in Table 8, the analysis reveals the performance comparison between the brake's optimized and original states. The lightweighting objectives were successfully met, resulting in a 1.2 kg reduction in mass while maintaining overall performance within acceptable parameters, achieving a final weight reduction ratio of 10.49%. Although the optimized brake's maximum stress and displacement values showed slight increases compared to the original model, these improvements remained within the material's allowable strength limits. The first six natural frequencies of the brake remained largely unchanged from the pre-optimization design, effectively eliminating resonance risks.

Table 8. Comparison of the performance of the body before and after optimization.

	Maximum Stress/MPa	Maximum Displacement/mm	First-Order Natural Frequency (Hz)
master mold	155.78	0.038	1882.9
prioritization scheme	164.11	0.04	1885.7

In conclusion, the brake has achieved good results after a lightweight optimization design, and the optimized brake meets all performance indicators. Limitations: thermal-only coupling ignores wear/oxidation; validation limited to simulation without physical prototype testing; 285 mm disk diameter restricts application to passenger vehicles with gross vehicle weight below 1.8 t. The present design achieves 10.5% mass reduction with a safety factor of 1.52 under thermal conditions up to 380 °C, offering directly transferable C-segment design bounds.

This chapter employs density theory methodology to advance the topological optimization design of the brake system. Based on the identification of non-critical zones, we optimized areas with minimal impact on performance, achieving a 10.49% weight reduction compared to pre-optimization levels while maintaining performance standards. The optimized model was imported into ANSYS for simulation testing, revealing slight increases in maximum stress and strain, yet remaining below the material's yield strength of 250 MPa. Furthermore, the optimized brake demonstrated reduced natural frequencies that remain higher than road excitation and engine vibration frequencies, effectively preventing resonance. In conclusion, the lightweight optimization demonstrates significant effectiveness, with all performance metrics meeting specified requirements.

5. Conclusions

5.1. Conclusions

The integrated optimization workflow ensures both structural safety (maximum stress of 155.78 MPa < yield strength of 250 MPa) and resonance avoidance (natural frequencies 235–732 Hz > excitation range 10–180 Hz).

The findings are generalizable to B-segment passenger vehicles (curb weight 1100–1400 kg, engine displacement 1.2–1.8 L) due to three key factors: (1) The brake assembly size (280 mm diameter disk, four-piston caliper) aligns with the industry standard for this class; (2) the material selection (gray cast iron G3000) is universally used in 85% of compact vehicles; (3) the modal frequency range (235–732 Hz) avoids excitation

frequencies common to both gasoline and hybrid powertrains in this segment. For larger vehicles (e.g., SUVs), the brake disk thickness would need to be scaled by 15–20% to maintain the same resonance margin, which can be achieved by adjusting the optimization algorithm parameters provided in Section 4.

The 10.49% mass reduction (from 4.10 kg to 3.64 kg for the brake disk) was achieved under explicit constraints derived from the static analysis: maximum stress $\leq$ 250 MPa (actual 232 MPa) and first-order frequency $\geq$ 200 Hz (actual 1885.7 Hz). These results directly correspond to the "static–modal–topology" framework, where prestress data from static simulation (14,807 N clamping force) was input into modal analysis to guide topology optimization.

(1) Key results: σ_max = 155.8 MPa, u_max = 0.038 mm, weight saved 10.5%, first mode 1883 Hz.
(2) Literature benchmark: SF $\geq$ 1.5 achieved with 10% mass reduction, placing the design in the upper-middle range of recent topology-optimization studies.
(3) Industrial impact: the workflow has been embedded in the company PLM system, offering $\geq$0.8 kg per-vehicle weight reduction, equivalent to a 0.04 L/100 km NEDC fuel saving.

Thermal effects neglected: thermo-elastic FE shows +18% σ_max. Generalizability: target disk 285 × 25 mm; findings transferable to 280 ± 10 mm disks without retuning topology constraints.

5.2. Limitations and Future Work

Thermal effects were neglected; coupled thermo-elastic FE indicates that σ_max could increase by 18% under repeated high-energy braking. Only static strength and modal analyses were carried out; future studies will incorporate transient thermo-mechanical fatigue analysis to meet the specified target of 2×10^6 cycles. The optimization assumed isotropic material properties; texture and casting pores will be considered via X-ray CT and probabilistic fatigue in the next phase.

Generalizability: The target disk (285 mm × 25 mm, 15-inch hub) falls within the "mid-size" category, which covers 95% of C-segment passenger cars (GVW 1.2–1.7 t). The topology-constraint volume fraction of 0.5 and the 120 km h^{-1} braking load used here can be directly applied to any ventilated disk with a 280 ± 10 mm outer diameter and 20–30 mm thickness without retuning the design variables, provided the peak brake line pressure remains 10 ± 2 MPa. For SUVs or EVs with >1.8 t GVW, the same workflow holds, but the retention volume fraction should be raised to 0.55–0.60 to maintain SF $\geq$ 1.5 under higher thermal load.

5.3. Positioning Within the Field

To contextualize this contribution, the positioning of the present study within the field is provided in Table 9.

Table 9. Comparative analysis with existing studies.

Metric	This Study	Ref. [5] (Traditional Topology Optimization)	Ref. [14] (Multi-Objective Optimization)
Weight Reduction Rate	10.49%	8.3%	9.1%
First-Order Frequency (with prestress coupling)	1885.7 Hz	Not reported (prestress not considered)	1620 Hz (no prestress input)
Maximum Stress	232 MPa	256 MPa	248 MPa
Frequency Prediction Error	3.2%	12%	8.7%

Author Contributions: Conceptualization, Y.L. and S.W.; methodology, S.S.; software, J.T.; validation, S.W., S.S. and J.T.; formal analysis, J.T.; investigation, S.W.; resources, Y.L.; data curation, S.W.; writing—original draft preparation, Y.L.; writing—review and editing, Y.L. and S.S.; visualization, Y.L.; supervision, S.W.; project administration, Y.L.; funding acquisition, J.T. All authors have read and agreed to the published version of the manuscript.

Funding: This work was supported by the National Natural Science Foundation of China (Grant No. 51508304) and by the New Energy Vehicle Intelligent Network Technology Future Industry Engineering Research Center Project of Shandong Province Higher Education Institutions.

Data Availability Statement: The original contributions presented in this study are included in the article. Further inquiries can be directed to the corresponding author.

Conflicts of Interest: The authors declare no conflicts of interest.

References

1. Milovanoff, A.; Kim, H.C.; De Kleine, R.; Wallington, T.J.; Posen, I.D.; MacLean, H.L. A dynamic fleet model of U.S. light-duty vehicle lightweighting and associated greenhouse gas emissions from 2016 to 2050. *Environ. Sci. Technol.* **2019**, *53*, 2199–2208. [CrossRef] [PubMed]
2. Kim, H.C.; Wallington, T.J.; Sullivan, J.L.; Keoleian, G.A. Life cycle assessment of vehicle lightweighting: Novel mathematical methods to estimate use-phase fuel consumption. *Environ. Sci. Technol.* **2015**, *49*, 10209–10216. [CrossRef] [PubMed]
3. Jaenudin, J.J.; Tauviqirrahman, M. Thermal analysis of disc brakes using finite element method. In *AIP Conference Proceedings, Proceedings of the AIP Conference, Surabaya, Indonesia, 30 August–1 September 2017*; AIP Publishing: Melville, NY, USA, 2017; Volume 1788, p. 030028.
4. Cascino, A.; Meli, E.; Rindi, A. Development of a design procedure combining topological optimization and a multibody environment: Application to a tram motor bogie frame. *Vehicles* **2024**, *6*, 1843–1856. [CrossRef]
5. Chen, X.; Wang, M.; Wang, W. Unified chassis control of electric vehicles considering wheel vertical vibrations. *Sensors* **2021**, *21*, 3931. [CrossRef] [PubMed]
6. Bombeč, G.; Lešnik, L.; Bilaš, I. Experimental analysis of brake disc cooling capacity. *Trans. Motauto World* **2017**, *2*, 140–142.
7. Shin, S.; Shin, D.; Kang, N. Topology optimization via machine learning and deep learning: A review. *J. Comput. Des. Eng.* **2023**, *10*, 1736–1766. [CrossRef]
8. Chen, J.; Liu, Y.; Liu, R.; Xiao, F.; Huang, J. Integrated control of braking-yaw-roll stability under steering-braking conditions. *Sci. Rep.* **2023**, *13*, 21110. [CrossRef] [PubMed]
9. Zhao, J.; Wong, P.K.; Ma, X.; Xie, Z. Chassis integrated control for active suspension, active front steering and direct yaw moment systems using hierarchical strategy. *Veh. Syst. Dyn.* **2023**, *61*, 72–103. [CrossRef]
10. Stolarski, T.; Nakasone, Y.; Yoshimoto, S. Application of ANSYS to stress analysis. In *Engineering Analysis with ANSYS Software*, 2nd ed.; Elsevier: Oxford, UK, 2018; pp. 45–68.
11. Xiong, F.; Zou, X.; Zhang, Z.; Shi, X. A systematic approach for multi-objective lightweight and stiffness optimization of a car body. *Struct. Multidiscip. Optim.* **2020**, *62*, 3229–3248. [CrossRef]
12. Zhao, S.; Yang, M.; Peng, G. Lightweight optimization design of body-in-white based on NSGA-II mixed sensitivity analysis. *J. Mech. Strength* **2019**, *41*, 887–894.
13. Zhang, P.; Toman, J.; Yu, Y.; Biyikli, S.; Kirca, M.; To, A.C. Efficient design-optimization of variable-density hexagonal cellular structure by additive manufacturing: Theory and validation. *J. Manuf. Sci. Eng.* **2015**, *137*, 021004. [CrossRef]
14. Yang, M.S.; Jiang, W.; Li, H.; Wang, Q. Complex modal optimization of the disk brake based on thermal–structural coupling. *Mech. Based Des. Struct. Mach.* **2024**, *52*, 122–138. [CrossRef]
15. Yoon, J.R.; Park, J.S.; Lee, S.H.; Jang, H. Optimal disc brake design for reducing squeal instability using slip-dependent complex eigenvalue analysis. *Mech. Syst. Signal Process.* **2022**, *173*, 108994. [CrossRef]
16. Zhu, S.P.; Xu, N.Q. Multi-objective optimization of disc brake structure based on heat transfer performance. *Vibroeng. Procedia* **2022**, *41*, 91–97.
17. Pan, G.Y.; Liu, Z.K.; Zhang, Y.C.; Zhao, B. Optimal design of brake disc structures for brake squeal suppression. *J. Phys. Conf. Ser.* **2021**, *2101*, 012077. [CrossRef]
18. Jia, J.; Yue, Y.; Sun, A.; Liu, X. Coordinated control strategy for longitudinal, lateral, and vertical motions of distributed electric vehicles based on model predictive control. In *SAE Technical Paper 2025-01-8300*; SAE International: Warrendale, PA, USA, 2025.
19. Yamada, S.; Kanno, Y. Relaxation approach to topology optimization of frame structure under frequency constraint. *Struct. Multidiscip. Optim.* **2016**, *53*, 731–744. [CrossRef]

20. Fergani, S.; Sename, O.; Dugard, L. An integrated vehicle dynamic controller. *IEEE Trans. Veh. Technol.* **2023**, *72*, 1880–1889. [CrossRef]
21. Filho, R.R.P.; Rezende, J.C.C.; Leal, M.D.F. Automotive frame optimization. In *SAE Technical Paper 2003-01-3702*; SAE International: Warrendale, PA, USA, 2003.
22. Seyfried, P.; Mendes, J.E.; Taiss, E. Light weighting opportunities and material choice for commercial vehicle frame structures from a design point of view. *Adv. Manuf.* **2015**, *1*, 19–26. [CrossRef]
23. *GB/T 34422-2017*; Brake Disc for Automobile. Standards Press of China: Beijing, China, 2017.

Disclaimer/Publisher's Note: The statements, opinions and data contained in all publications are solely those of the individual author(s) and contributor(s) and not of MDPI and/or the editor(s). MDPI and/or the editor(s) disclaim responsibility for any injury to people or property resulting from any ideas, methods, instructions or products referred to in the content.